J. Phys. Earth, **44**, 701–711, 1996

Complex Structure of Mantle Discontinuities at the Tip of the Subducting Slab beneath Northeast China

—A Preliminary Investigation of Broadband Receiver Functions—

Fenglin Niu* and Hitoshi Kawakatsu

Earthquake Research Institute, The University of Tokyo, Bunkyo-ku, Tokyo 113, Japan

Broadband seismic waveform data recorded at stations in the western Pacific region are analyzed to investigate mantle discontinuities. By using teleseismic deep events, we observe unambiguous P-to-S conversion waves associated with the mid-mantle discontinuities in many of the individual seismograms. The commonly used method of stacking receiver functions is not so effective in this case due to the limited number of deep events. An inversion scheme is developed to determine a discontinuity response function at each station by fitting observed waveform data with superpositions of the P-to-S converted waves. Beneath the station in northeast China (MDJ) where the subducted Pacific plate appears to stagnate along the "660-km" discontinuity, the discontinuity response function has more complicated features than those of other stations. The preliminary results indicate no depression of the "660-km" discontinuity at the tip of the subducting slab beneath MDJ; instead a multiple-discontinuity structure down to a depth of 780 km is observed.

1. Introduction

In spite of the large number of studies performed on seismic mantle discontinuities, the physical nature of these discontinuities is still controversial. They can be related either to phase transitions or to compositional boundaries. The difference between the two physical models may be discriminated by accurate seismic observations of the discontinuities; for example, the behavior of the "660-km" discontinuity adjacent to a subducting slab (Ito *et al.*, 1990; Kincaid and Olson, 1987) or the sharpness of discontinuities (Ito and Takahashi, 1989; Katsura and Ito, 1989). Although studies of mantle discontinuities using long-period SS precursors by Shearer and Masters (1992) and Shearer (1993) provide a well-covered global observation of the "410-km" and "660-km" discontinuities, it is insufficient to resolve "local" velocity structures near subducting slabs. Recent studies (e.g., Paulssen, 1988; Bock and Ha, 1984; Richards and Wicks, 1990; Mizuta *et al.*, 1991; Vidale and Benz, 1992; Wicks and Richards, 1993; Niu and Kawakatsu, 1995) show that analysis of short-period reflected and/or converted waves at upper-mantle discontinuities is an effective method to obtain detailed information about these discontinuities. A serious drawback of reflected- and converted-wave observations is that these phases are generally of low amplitude, which makes it difficult to identify them.

In this study, we investigate the behavior of the "660-km" discontinuity adjacent to a subducting slab by identifying near-station P-to-S converted waves (hereafter referred to as P660s) from teleseismic events. As shown in Fig. 1, P660s travels almost the same ray path as that of the direct P-wave before it converts to an S-wave at the "660-km" discontinuity just beneath the station. The travel-time difference between these two phases depends on the local depth of the "660-km" discontinuity. A variation of the estimated source depth has almost no effect on this time difference, and we use this time difference to estimate the depth of conversions. P660s has the polarization of teleseismic SV motion. It has an amplitude of several percent compared to that of the direct P-wave (we assume the *iasp91* seismic velocity model, Kennett and Engdahl, 1991). The relative amplitude to the direct P-wave is mainly determined by the impedance contrast at the discontinuity and is hardly affected

Received September 21, 1995; Accepted November 29, 1995

* To whom correspondence should be addressed.

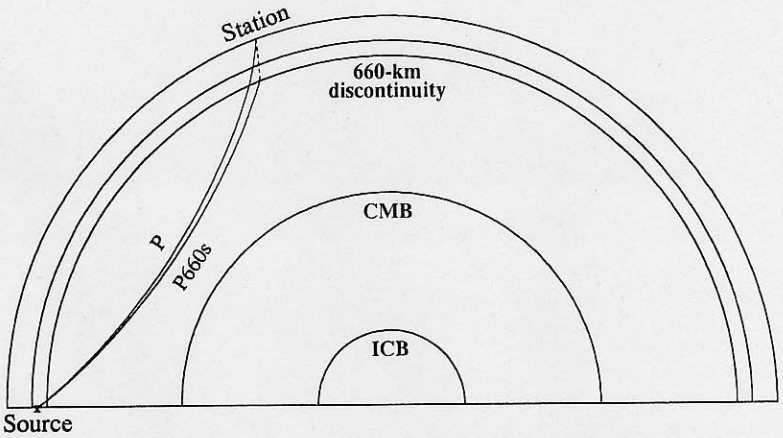

Fig. 1. Schematic illustration of ray paths of the direct P-wave and a P-to-S converted wave at a mantle discontinuity (P660s) beneath a station. The converted wave travels almost the same ray path as that of the direct P-wave before it converts to S-wave at the "660-km" discontinuity just beneath the station.

by the source mechanism. So once an effective method is devised to analyze the near-station P-to-S conversion waves, it may be used to investigate the nature of mantle discontinuities globally, as well as locally.

Previous studies on the P660s phase show that there are a great variety of amplitudes observed. Even in the same NARS array, Paulssen (1985, 1988) observed an anomalously high-amplitude P660s phase in both individual seismograms and stacked waveforms, while van der Lee *et al.* (1994) found no clear P660s signals in any individual seismogram and just weak energy in the stacked waveforms. Motivated by these apparently inconsistent observations and the recent availability of high-quality broadband data, we have carried out this study of the P660s phase using broadband data recorded at stations in the western Pacific region. We use only seismograms of deep events to get a better S/N ratio. As a result, we find a clear P660s phase in many individual seismograms (Fig. 2).

A radial component seismogram deconvolved with the corresponding vertical component P-wave is usually referred to as a receiver function when used in the study of crustal and lithospheric structures (e.g., Langston, 1979; Owens *et al.*, 1984; Kind *et al.*, 1995). A well-used method to improve the S/N ratio is the stacking of a large number of receiver functions. However, under the circumstances that only a small number of seismograms with a good S/N ratio are available, methods of waveform-fitting are more effective. In this paper, we introduce a waveform-fitting scheme to retrieve the signature of mantle discontinuities in receiver functions, and give some preliminary interpretation for the mantle structure beneath 3 stations in the western Pacific, MAJO (Matsushiro, Japan), MDJ (Mudanjiang, China), and HIA (Hailar, China). As shown in Fig. 3, the Pacific plate starts penetrating at the Japan trench and extends west to just beneath the northeastern part of China. The depth variation of the "660-km" discontinuity beneath MAJO, MDJ, and HIA, if present, therefore provides a direct assessment of the slab effect on the "660-km" discontinuity.

2. Data Selection

As we try to identify the very weak signal of P660s (P410s), we must ensure that there are no primary phases arriving in the same time window (approximately 35–75 s after the direct P-wave) of seismograms. That is, we do not expect the weak P660s (P410s) phase to be interferred by primary phases such as PP and PcP. For this purpose, we choose teleseismic events with an epicentral distance of 60–90°. To avoid further interference with pP and sP, we limited hypocentral depths to be deeper than ~400 km.

We use broadband data from the IRIS Data Management Center and the POSEIDON Data Center for deep events that occurred in the Tonga subduction zone. The coverage period is from January 1990 to December 1994, and the magnitude (M_w) of events is ≥ 5.6 (Table 1). There are a total of 24 deep events with a depth $\geq \sim 400$ km. To map the depth variation of the "660-km" discontinuity, we analyze data recorded at stations MAJO , MDJ, and HIA (Fig. 3).

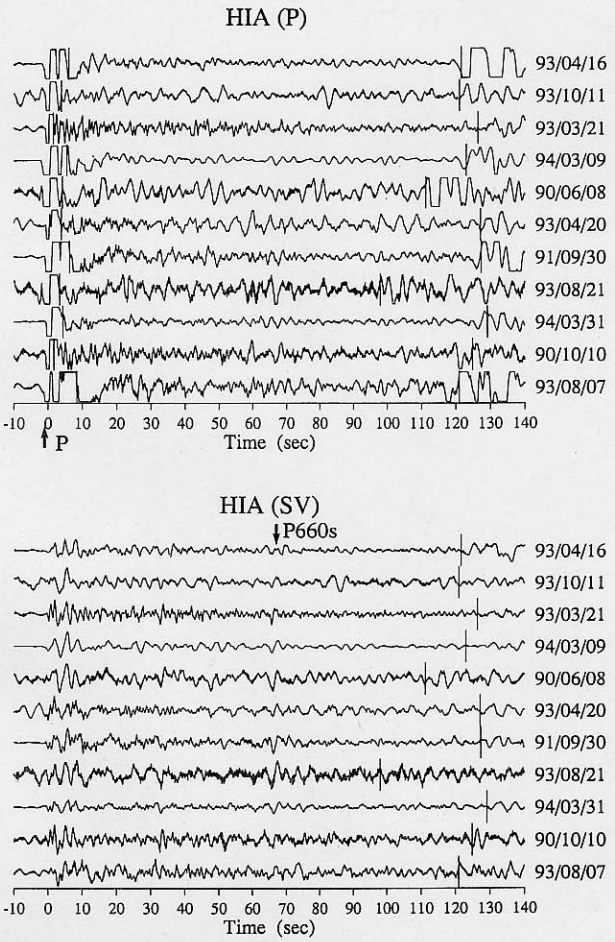

Fig. 2. Original P (top) and SV (bottom) seismograms of 11 deep events that occurred in the Tonga subduction zone recorded at station HIA (plotted from north to south). They are aligned so that the peak of the direct P seismogram occurs at time zero and is shown in the same scale. Vertical lines show the theoretical pP arrivals. The arrival time of P660s is indicated by the arrow.

3. Analysis Methods

Following Vinnik (1977), we first assume that the ray path of P660s stays in the great circle plane, which contains both the source and receiver, and rotate the two horizontal components (NS, EW) to the radial and transverse components. We then plot the particle motion for the first few cycles of the P-wave to determine the principal direction of the P motion. To detect the SV-wave, we further project the vertical and radial components in the principal direction of the P-motion and its perpendicular direction, which we refer to as the P and SV components, respectively. We mainly analyze the SV component in this study.

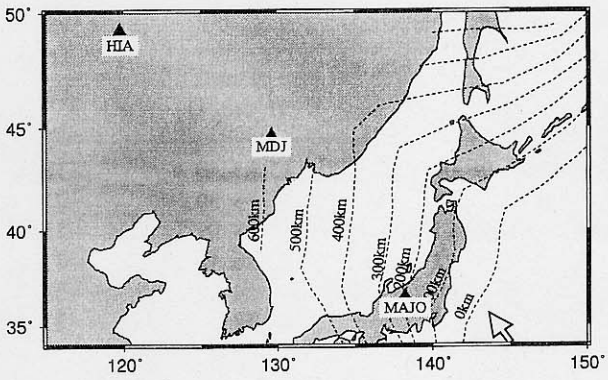

Fig. 3. Geographic distribution of the investigated broadband stations in this study. Dashed lines represent the deep seismicity in kilometers. The great circle arc, which connects the three stations and the epicentral region, share almost the same plane and is shown here by an arrow.

3.1. *Stacking of receiver functions*

The SV component is first deconvolved with the first few cycles of the direct P-wave (usually 10 s long) to produce a receiver function (Langston, 1979; Owens *et al.*, 1984). This process is to eliminate the difference of waveforms existing in different events. We then stack the receiver functions of different events to improve the S/N ratio. As noted in the previous section, the event depth has almost no influence on the travel-time delay of P660s (P410s) with respect to the direct P-wave. It is convenient to treat different events as an array (event array). The linear stacking process (e.g., Kanasewich, 1973) can be used for this purpose. We align the receiver functions such that the peak of deconvolved P-seismograms, which are normalized to unity, occurs at time zero. Next, the slowness for each stack is varied with respect to that of the direct P arrivals (defined as zero) in increments of 0.05 s deg^{-1} within the range of ± 1 s deg^{-1}. Because we stack only about 10 receiver functions for each station and because all the events are distributed in the same Tonga subduction zone, the stacking method is not so effective for raising the S/N ratio and the resolution of slowness for phases is relatively poor. For these reasons, we introduce the following inversion scheme to effectively retrieve the signature of mantle discontinuities from broadband receiver functions.

Table 1. Earthquakes.

Date (year min day)	Time (h min s)	Lat.	Lon.	Depth (PDE)	Mag. (M_w)	Stn.*
1990 06 08	15 05 10.2	−18.70	181.10	503.5	6.4	HIA
1990 06 26	12 08 30.2	−21.97	180.48	613.8	6.2	None
1990 07 11	19 48 09.5	−25.22	178.22	596.4	6.0	None
1990 07 22	09 26 18.0	−23.48	179.93	559.2	6.3	HIA
1990 10 10	05 54 58.0	−23.35	178.87	575.1	6.0	HIA MAJO
1990 11 29	20 58 11.7	−27.81	180.06	425.7	6.0	None
1991 09 30	00 21 47.5	−20.97	181.39	589.7	6.9	HIA MAJO
1991 12 03	10 33 42.0	−26.31	178.57	574.5	6.3	None
1992 07 11	10 44 20.9	−22.28	181.49	393.8	7.2	All
1992 08 30	20 09 06.9	−17.74	181.23	574.2	6.4	MAJO
1992 11 12	22 28 58.4	−22.35	181.92	378.5	6.2	All
1993 03 21	05 04 59.0	−17.70	−178.80	590.0	6.3	All
1993 04 16	14 08 40.0	−17.40	−178.90	563.0	6.9	All
1993 04 20	16 26 20.0	−20.40	−179.00	590.0	6.0	HIA MDJ
1993 08 07	17 53 28.5	−23.60	179.10	553.0	6.7	All
1993 08 21	09 42 37.0	−21.00	−178.20	430.0	6.1	All
1993 10 11	13 07 31.0	−17.40	−179.10	560.0	6.0	All
1994 03 09	23 28 07.6	−17.70	−178.60	570.0	7.6	All
1994 03 31	22 40 55.0	−21.70	−179.70	600.0	6.5	All
1994 10 27	22 20 31.0	−25.60	179.10	550.0	6.6	MAJO
1994 12 18	20 38 32.2	−17.70	181.00	550.0	5.6	MAJO
1995 01 17	16 54 11.7	−20.80	−179.40	640.0	6.3	MAJO

* None: no data for all the three stations; All: data are available for all the three stations.

3.2. Inversion of "discontinuity response function"

Figure 4(a) shows theoretical P and SV seismograms calculated for the *iasp91* model when a P plane wave arrives at a station from below with an incident angle of 35°, which corresponds to the approximate incident angle of P-waves arriving from Tonga to the stations of interest. The Thomson-Haskell method (Haskell, 1962) is used to construct synthetics, and the direct P-wave waveform of the event 94/03/09 is used as the incident P-wave. We notice that the first ~30 s part after the direct P-wave in the SV-seismogram is mainly contaminated by crustal reverberations. However, between ~30 s after the direct P-wave and the arrival of pP (about 100–130 s), signals are mainly associated with P-to-S conversion waves at the mantle discontinuities (P660s and P410s arrive at about 66 and 43 s, respectively). Therefore, we represent the observed SV waveforms within this time window in terms of the P-to-S converted waves at the mantle discontinuities.

For a discontinuity at the depth Z_i with the P-to-S transmission coefficient r_i, we first calculate the arrival time t_i of the P-to-S converted wave using the geometrical ray theory. The synthetic SV seismogram is given by a superposition of P-to-S converted waves at mantle discontinuities:

$$Syn^j(t) = \sum_{i=1}^{M} S^j(t - t_i^j) \cdot r_i \,, \tag{1}$$

where $S^j(t)$ is the source time function of jth event estimated from the P seismogram and M is the total number of discontinuities. By fitting the synthetic seismograms ($Syn^j(t)$) to the observed SV seismograms ($u^j(t)$) within appropriate time windows for all the events recorded at a station, we obtain the following equation to solve:

$$\boldsymbol{u} = \boldsymbol{S} \cdot \boldsymbol{r} \,. \tag{2}$$

Following Revenaugh and Jordan (1989), we call the sequence of the transmission coefficient (r_i) "discontinuity response function" (hereafter referred to as DRF) beneath a station. The DRF is calculated at every 2 km in the depth range between 300 and 900 km. The solution ($\hat{\boldsymbol{r}}$) of Eq. (2) may be obtained by multiplying the generalized inverse

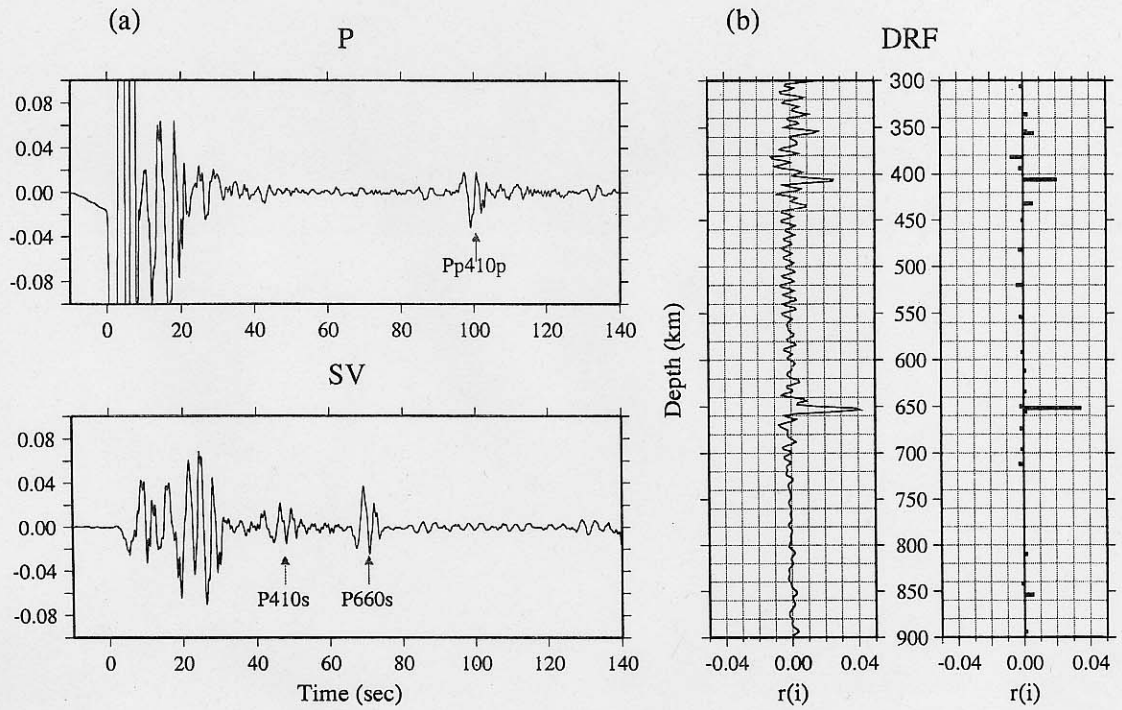

Fig. 4. (a) Synthetic P (top) and SV seismograms (bottom) calculated with the Thomson-Haskell method (see text for more details). Note that for the case of a noise-free seismogram, P-to-S converted phases at the mid-mantle discontinuities appear in the SV seismogram with appreciable amplitudes. (b) Discontinuity response functions estimated through the generalized (left) and recursive (right) inversions for the synthetic SV seismogram shown in (a); the P-to-S transmission coefficient is given as a function of the conversion depth.

operator (e.g., Aki and Richards, 1980) with the data ($\boldsymbol{u}$):

$$\hat{\boldsymbol{r}} = \boldsymbol{S}_{\mathrm{g}}^{-1} \cdot \boldsymbol{u} \,. \tag{3}$$

A similar approach was recently taken independently by Gurrola *et al.* (1995) to investigate the shallow structure beneath stations from receiver functions.

A DRF can be also obtained by a more intuitive method suggested by Kikuchi and Kanamori (1982) to determine the complex multiple-shock sequence of earthquake sources. We first determine the transmission coefficient (r_1) and the depth (Z_1) in Eq. (1) by minimizing the residual defined by

$$\Delta_1 = \int_{T_1}^{T_2} \sum_{j=1}^{L} [u^j(t) - r_1 S^j(t - t_1^j)]^2 \mathrm{d}t \,, \tag{4}$$

where T_1–T_2 is the investigated time window; L is the total number of events recorded at a station; t_1^j is the travel time difference between the P-to-S converted wave at the discontinuity of depth Z_1 and the direct P-wave for the jth event. From Eq. (4), we find that Δ_1 is minimized if

$$\sum_{j=1}^{L} \int_{T_1}^{T_2} u^j(t) S_j(t - t_1^j) \mathrm{d}t = \text{maximum} \,, \tag{5}$$

$$r_1 = \frac{\sum_{j=1}^{L} \int_{T_1}^{T_2} u^j(t) S^j(t - t_1^j) \mathrm{d}t}{\sum_{j=1}^{L} \int_{T_1}^{T_2} S^j(t) S^j(t) \mathrm{d}t} \,. \tag{6}$$

Next we apply the above procedure to the residual waveforms

$$u'^j(t) = u^j(t) - r_1 S^j(t - t_1^j) \,, \tag{7}$$

and determine the second values Z_2 and r_2. The above procedure is repeated until no more significant decrease in the residual occurs. Since this method searches for the single discontinuity depth and its transmission coefficient that can most improve the fit to the data in each iteration, a "spiky" DRF is usually produced, although it does not necessarily

mean that the actual discontinuity is as sharp as seen in a DRF.

The generalized inverse solution and the iteration result for the Thomson-Haskell synthetic SV seismogram shown in Fig. 4(a) are depicted in Fig. 4(b). The two peaks near 410 and 660 km correspond to the two discontinuities of the *iasp91* model at those depths. Since the first ~30 or ~40 s (the exact time is determined by the depth of the Moho) part after the direct P-wave in the SV seismogram is highly contaminated by crustal reverberations, artificial structures may appear in the shallow part of the DRF produced (such as the peak around 350 km in Fig. 4(b)). However, for depths below 550 km, the DRF is especially clear. For a noise-free SV seismogram, the possible existing discontinuities can be detected by these inversion schemes. However, for real seismograms with various sorts of noise, many artificial structures may appear in the DRF. In this paper, we only discuss the most prominent structure in the DRF, which corresponds to the "660-km" discontinuity. In the following text, we will only show the DRF in the depth range of 600–800 km, corresponding to the P-to-S arrival in the time window approximately 60–80 s after the direct P-wave.

4. Observation of the Mantle Discontinuities

Seismograms recorded at station HIA had the best S/N ratio among the three investigated stations. Of the total of 24 deep events occurring in Tonga during the analyzed period, 14 were recorded at HIA, among which the seismograms of 11 events show relatively favorable S/N ratios (Fig. 2). We expect to see the mantle structure beneath a typical continent from the analysis of the seismograms recorded at this station. A very strong peak at the depth of about 660 km is observed in the DRF (Fig. 5), which corresponds to the well lined-up phase at ~66 s in the SV seismograms shown in Fig. 2. After inversion, about 60–90% of the residual is reduced. In Fig. 6, we show the synthetic seismograms together with observed waveforms for some typical events.

The amplitude of the P-to-S transmission coefficient of the phase at the "660-km" discontinuity is approximately 0.09, much larger than that (~0.04, Fig. 4) of the *iasp91* model, which has a velocity contrast of 5.8% and a density contrast of 7.6% across the "660-km" discontinuity. The amplitude of the P-to-S conversion coefficient at a

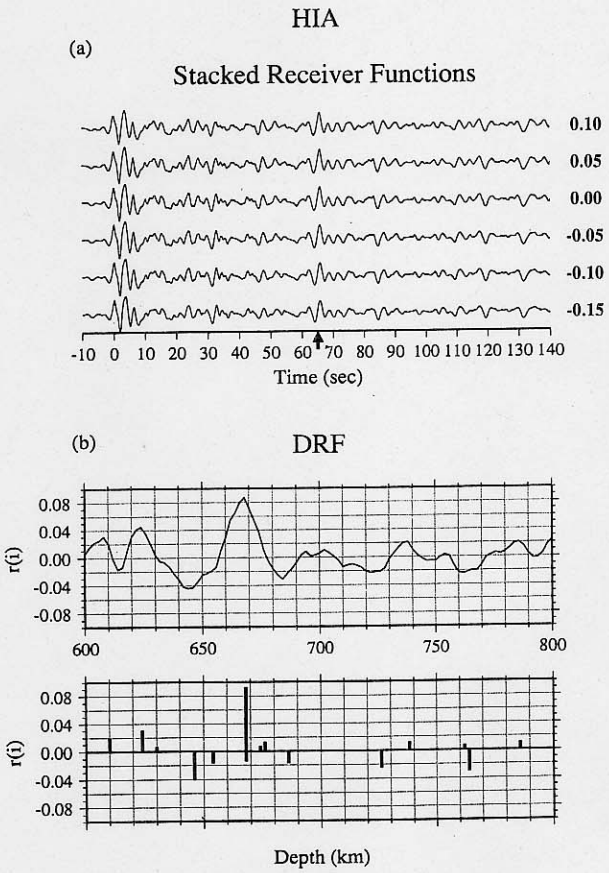

Fig. 5. (a) Stacked broadband receiver functions at station HIA. Numbers at the right side indicate the slowness relative to that of the direct P-wave (defined as zero) used in stacking. The arrow on the axis indicates the theoretical arrival time of the P660s phase. (b) The DRF beneath station HIA; conventions are the same as in Fig. 4(b).

discontinuity is mainly determined by the S-wave velocity jump. The observed large amplitude may therefore suggest a large S-wave velocity jump across the "660-km" discontinuity beneath the station HIA. Since a discontinuity with a dipping structure could introduce a factor of two increase in the amplitude of the P-to-S converted wave, it might be that the "660-km" discontinuity beneath station HIA dips eastward at an angle of approximately 30°. However, considering that the observed amplitude is more than twice the synthetic value, we should not simply interpret it as the effect of the "660-km" discontinuity alone. The shallow structure beneath HIA, the focusing effect of the discontinuity and the overlap with other reverberative signals may also be partially responsible for the observed large amplitude.

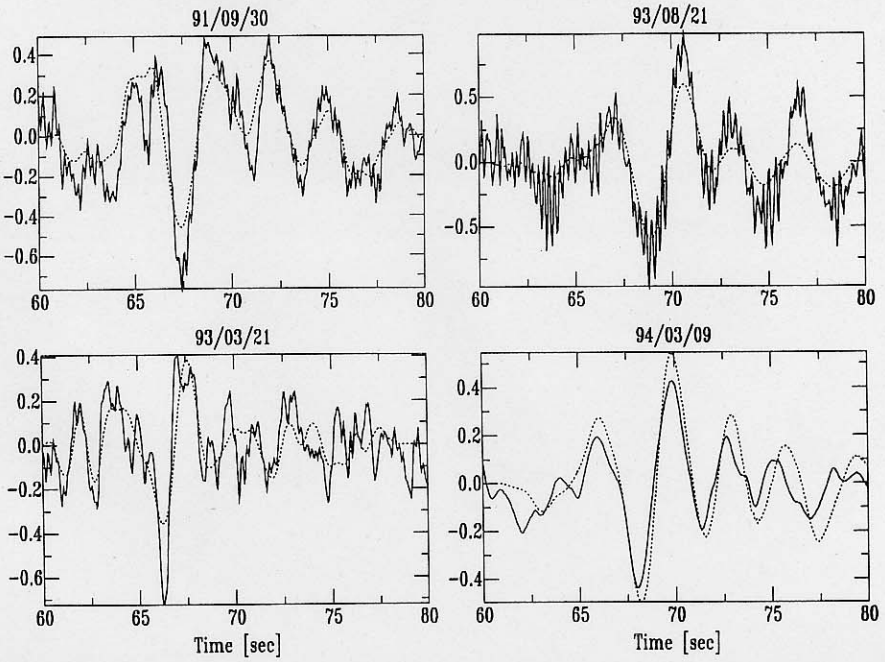

Fig. 6. Synthetic SV seismograms of some events (dotted lines) at station HIA are plotted against observed waveforms (solid lines). About 60–90% of the residual is usually reduced after inversion. In the depth range of 600–800 km, P-to-S converted waves arrive in the time window approximately 60–80 s after the direct P-wave.

In Fig. 5, we can also see several other signals at about 31, 46, and 85 s in the stacked receiver functions, possibly corresponding to discontinuities at depths of approximately 300, 450, and 920 km, respectively. However, as we noted in the previous section, noises may also produce such features due to the small number of seismograms; further accumulation of data and/or further improvement in the investigation method are required to give a conclusive interpretation of these signals.

For the northeast China station, MDJ, waveform data of 10 events are available, among which seismograms of 7 events are used in the inversion (Fig. 7). In Fig. 7, we can see several signals between 65 and 80 s in the seismograms of all 7 events. The stacked broadband receiver functions and the results of DRF inversion are shown in Fig. 8. The inversion results are generally in good agreement with the stacked broadband receiver functions. However, we can obtain a more detailed structure from the DRF; for example, the complicated signals in the stacked receiver functions at about 75 s correspond to two major peaks in the DRF. Figure 8 indicates that the discontinuity structure beneath MDJ is very complicated; there are 3 impedance increases observed at depths about 670, 740, and 780 km. The P-to-S transmission coefficients of these 3 discontinuities suggest that they have approximately the same impedance contrast as that of the "660-km" discontinuity of the *iasp91* model.

Seismograms recorded at station MAJO generally contain much noise, which may be partially due to the complicated structure beneath Japan. There are a total of 11 SV seismograms which have a relatively good S/N ratio. No systemic signal lines up so unambiguously as to be interpreted as a P-to-S conversion wave at the mantle discontinuities in the individual seismograms. However, a signal corresponding to P660s may be recognized in the stacked receiver functions (Fig. 9(a)), even though it is almost on the noise level. The corresponding peak in DRF is located approximately at a depth of 660 km (Fig. 9(b)).

5. Discussion

One of the advantages of analyzing near-station P-to-S conversion phases is that the depth of the discontinuity determined by the present method is insensitive to a source mislocation and/or the effect of the velocity heterogeneity in the source region, which are the main uncertainties in determining the depth of the "660-km" discontinuity using the

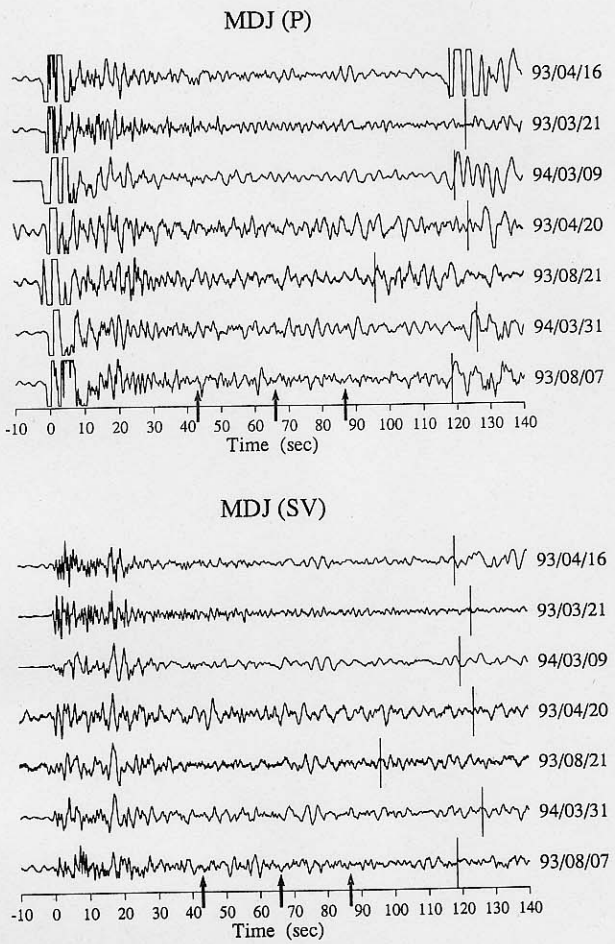

Fig. 7. Same as Fig. 2 for station MDJ. Arrows on the axis indicate theoretical arrival times for the P-to-S converted waves at mid-mantle discontinuities (from left to right: "410-km," "660-km," "920-km").

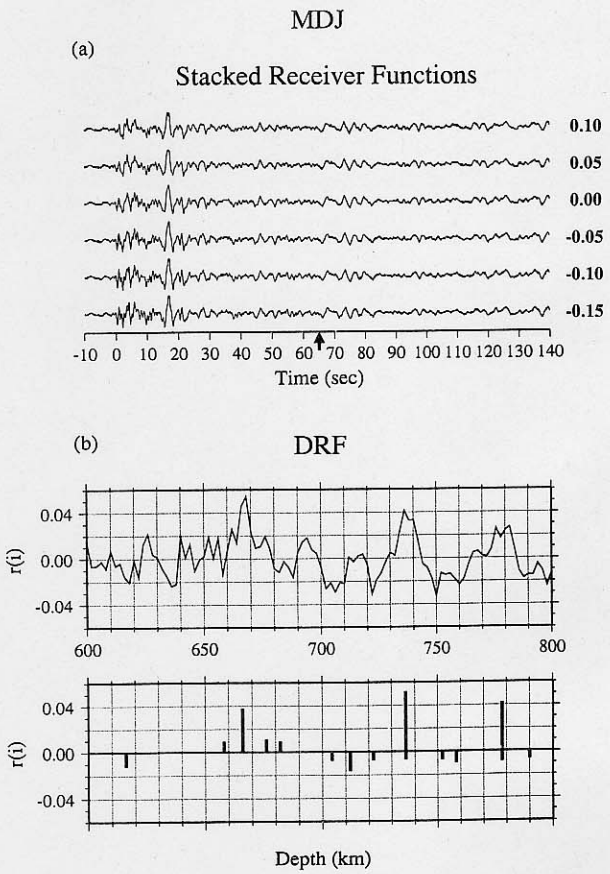

Fig. 8. Same as Fig. 5 for station MDJ.

near-source S-to-P conversion wave method (Bock and Ha, 1984; Richards and Wicks, 1990; Mizuta *et al.*, 1991; Vidale and Benz, 1992; Wicks and Richards, 1993; Niu and Kawakatsu, 1995). The observed difference between the P-wave and P660s arrivals is determined by the S–P time between the discontinuity and the surface. Therefore, the main error which may occur in determining the depth of the discontinuity by this method is the velocity heterogeneity (especially the S-wave heterogeneity). For the two extreme regions, the tectonic and shield regions studied by Grand and Helmberger (1984), Walck (1984) and Lefevre and Helmberger (1989), the S–P time difference due to the velocity heterogeneity is as much as 4 s, which leads to an error of approximately 40 km for the estimated depth of the "660-km" discontinuity. However, a P-wave tomographic study by van der Hilst *et al.* (1991) suggests that the velocity heterogeneity of the upper mantle in the studied region is not so strong; only a 0.5% lower velocity anomaly was observed beneath station MDJ. As no detailed S-wave structure models can be referred to in the same region, if we assume that the S-wave velocity heterogeneity is not so different from that of the P-wave (that is, we assume that $\delta V_S/V_S \simeq \delta V_P/V_P$), then the anomaly on S–P time due to the velocity heterogeneity will be less than 1 s (10 km in depth). Therefore, the velocity heterogeneity should not affect our results severely.

To confirm the broadband results, we also apply band-pass filtering to the original broadband receiver functions at several period bands (0.5–2, 2–5, and 5–10 s), and find that the receiver functions have relatively good S/N ratios in the 2–5 s period band; for stations MAJO and HIA, the results of band-pass filtered data are basically consistent with that inferred from the broadband analysis. However, a

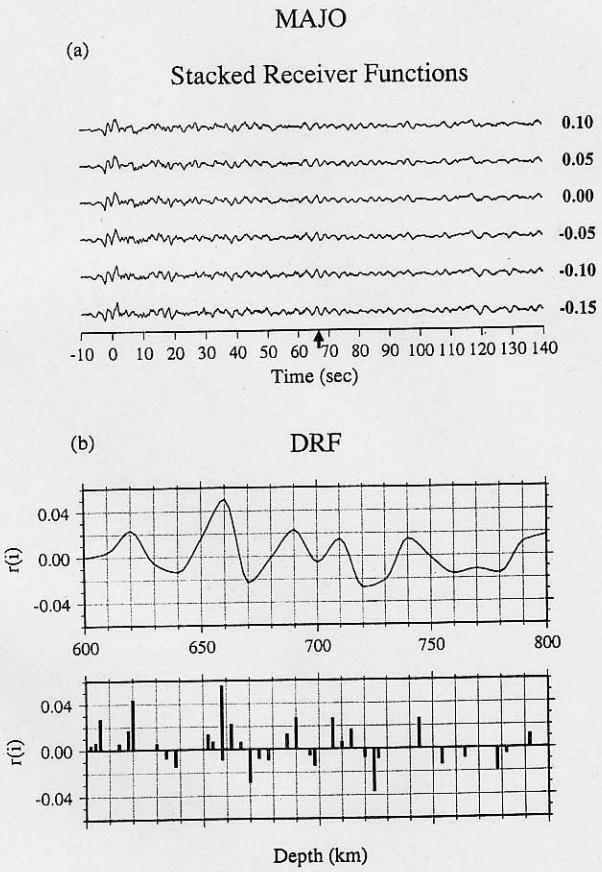

Fig. 9. Same as Fig. 5 for station MAJO.

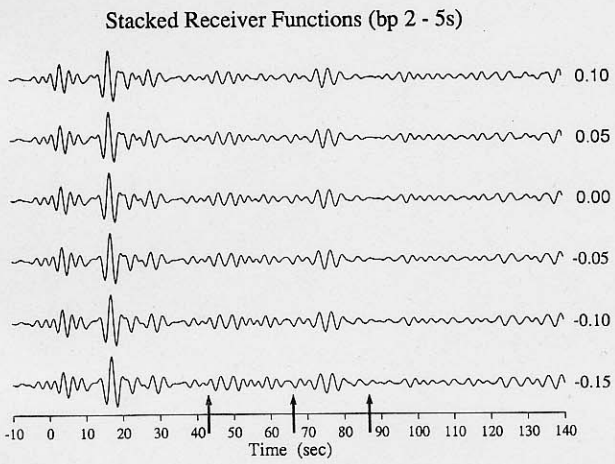

Fig. 10. Stacked receiver functions at station MDJ in the period range 2–5 s. Conventions are the same as in Fig. 7.

significant difference between band-pass filtered stacked receiver functions (Fig. 10) and the broadband ones (Fig. 8) is observed at station MDJ; in contrast to the complicated waveform between

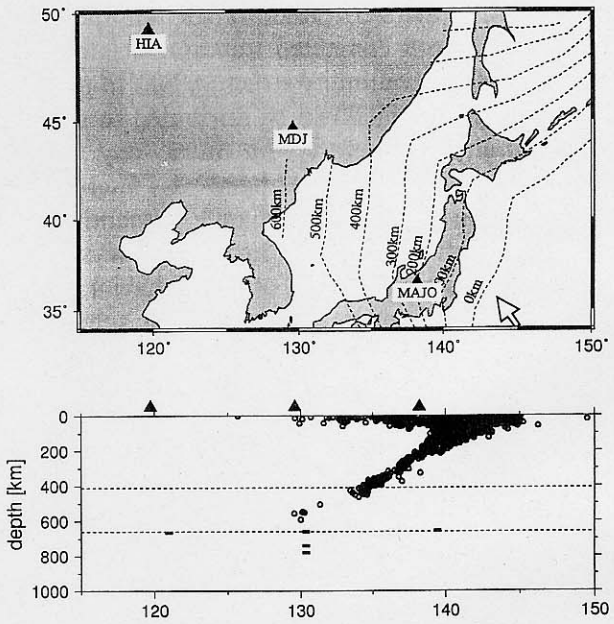

Fig. 11. (Top) Geographic distribution of the investigated broadband stations in this study. (Bottom) Depth of the mantle discontinuities beneath the 3 investigated stations. Earthquake locations from the International Seismological Center (ISC) from 1964 to 1991 are also shown. These earthquakes define the Wadati-Benioff zone which outlines the position of the subducting Pacific slab.

65 and 80 s observed in Fig. 8(a), we see only one signal at about 72 s, which may be interpreted as a single discontinuity at the depth of about 720 km. This discrepancy leads to very different interpretations for the mantle discontinuity structure beneath the station. The band-pass filtered data suggest that the "660-km" discontinuity is depressed as much as 60 km beneath MDJ, where the subducting Pacific plate stagnates along the "660-km" discontinuity (Fukao *et al.*, 1992). This observation is apparently consistent with those of previous studies (Shearer and Masters, 1992; Shearer, 1993; Vidale and Benz, 1992; Wicks and Richards, 1993; Niu and Kawakatsu, 1995) in the sense that the "660-km" discontinuity is depressed in the vicinity of subduction slabs, although the 60 km slab-induced deflection is close to the upper limit of values that have been observed. Meanwhile, the broadband waveforms indicate that there may be no depression of the "660-km" discontinuity, rather that a multiple-discontinuity structure down to the depth of 780 km exists at the tip of the subducting slab. It

seems that in the 2–5 s period range the superposed signals of P-to-S converted waves associated with the multiple-discontinuity structure bias to produce a simple phase which can be attributed to a single discontinuity. Therefore, we must pay special attention when we interpret band-pass filtered data to infer the structure of mantle discontinuities. Further careful analyses of broadband waveforms may reveal a new picture of the behavior of the mantle discontinuities associated with subducting slabs, and threfore provide a new understanding of the physical nature of mid-mantle discontinuities.

The suggestion of a complex mantle structure beneath northeast China can also be found in the recent multiple-ScS reverberations study by Revenaugh and Sipkin (1994). A comparison with the structures beneath stations MAJO and HIA, which represent different tectonic regions (Fig. 11), shows that this phenomena is limited only at the tip of the subducting Pacific slab. Consequently, the complex structure is a kind of "slab effect" on the "660-km" discontinuity, although there is no clear mineralogical explanation for it at the moment.

6. Conclusion

The ongoing expansion of broadband seismometers all over the world has enabled the accumulation of a great amount of high-quality data. The main purpose of this study is to devise a method to map mid-mantle discontinuities globally. In this paper, we present preliminary results after investigating the data of stations located in the western Pacific region. Although this is far from a global examination of mantle discontinuities at present, we have shown that it is possible to determine the depth of mantle discontinuities beneath a station with reasonable precision by analyzing broadband waveforms, and that the structure of mantle discontinuities at the tip of a subducting slab may be much more complicated than previously thought.

We are grateful to the POSEIDON Data Center and the IRIS Data Management Center for supplying data. We also thank Dr. H. Fujisawa for discussion, and Dr. Peter Shearer for constructive review.

REFERENCES

Aki, K. and P. G. Richards, *Quantitative Seismology: Theory and Methods*, W. H. Freeman, San Francisco, Vol. 2, 932 pp., 1980.

Bock, G. and J. Ha, Short-period S–P conversion in the mantle at a depth near 700 km, *Geophys. J. R. Astron. Soc.*, **77**, 593–615, 1984.

Fukao, Y., M. Obayashi, M. Inoue, and M. Nenbai, Subducting slabs stagnant in the mantle transition zone, *J. Geophys. Res.*, **97**, 4809–4822, 1992.

Grand, S. P. and D. V. Helmberger, Upper mantle shear structure of the North America, *Geophys. J. R. Astron. Soc.*, **76**, 399–438, 1984.

Gurrola, H., G. E. Baker, and J. B. Minster, Simultaneous time-domain deconvolution with application to the computation of receiver functions, *Geophys. J. Int.*, **120**, 537–543, 1995.

Ito E. and E. Takahashi, Postspinel transformations in system Mg_2SiO_4–Fe_2SiO_4 and some geophysical implications, *J. Geophys. Res.*, **94**, 10637–10646, 1989.

Ito., E., M. Akaogi, L. Topor, and A. Navrotsky, Negative pressure-temperature slopes for reactions forming $MgSiO_3$ perovskite from calorimetry, *Science*, **249**, 1275–1278, 1990.

Haskell, N. A., Crustal reflections of the plane P and SV waves, *J. Geophys. Res.*, **67**, 4751–4767, 1962.

Kanasewich, E. R., *Time Sequence Analysis in Geophysics*, The University of Alberta Press, Edmonton, 364 pp., 1973.

Katsura, T. and E. Ito, The system Mg_2SiO_4–Fe_2SiO_4 at high pressures and temperatures: Precise determination of stabilities of olivine, modified spinel, and spinel, *J. Geophys. Res.*, **94**, 15663–15670, 1989.

Kennett, B. L. N. and E. R. Engdahl, Travel times for global earthquake location and phase identification, *Geophys. J. Int.*, **105**, 429–465, 1991.

Kikuchi, M. and H. Kanamori, Inversion of complex body waves, *Bull. Seismol. Soc. Am.*, **72**, 491–506, 1982.

Kincaid, C. and P. Olson, An experimental study of subduction and slab migration, *J. Geophys. Res.*, **92**, 13832–13840, 1987.

Kind, R., G. L. Kosarev, and N. V. Petersen, Receiver function at the stations of the German Regional Seismic Network (GRSN), *Geophys. J. Int.*, **121**, 191–202, 1995.

Langston C. A., Structure under Mount Rainier, Washington, inferred from teleseismic body waves, *J. Geophys. Res.*, **84**, 4749–4762, 1979.

Lefevre, L. V. and D. V. Helmberger, Upper mantle P velocity structure of the Canadian Shield, *J. Geophys. Res.*, **94**, 17749–17765, 1989.

Mizuta, S., Y. Morita, and H. Hamaguchi, 670 km discontinuity beneath Fiji region (1), Program and Abstracts, Seismol. Soc. Japan, 2, 189, 1991 (in Japanese).

Niu F. L. and H. Kawakatsu, Direct evidence for the undulation of the 660-km discontinuity beneath Tonga: Comparison of Japan and California array data,

Geophys. Res. Lett., **22**, 531–534, 1995.

Owens T. J., G. Zandt, and S. R. Taylor, Seismic evidence for an ancient rift beneath the Cumberland plateau, Tennessee: A detailed analysis of broadband teleseismic P waveforms, *J. Geophys. Res.*, **89**, 7783–7795, 1984.

Paulssen, H., Upper mantle converted waves beneath the NARS array, *Geophys. Res. Lett.*, **12**, 709–712, 1985.

Paulssen, H., Evidence for a sharp 670-km discontinuity as inferred from P-to-S converted waves, *J. Geophys. Res.*, **93**, 10489–10500, 1988.

Revenaugh, J. and T. H. Jordan, A study of mantle layering beneath the western Pacific, *J. Geophys. Res.*, **94**, 5787–5813, 1989.

Revenaugh, J. and S. A. Sipkin, Mantle discontinuity structure beneath China, *J. Geophys. Res.*, **99**, 21911–21927, 1994.

Richards, M. A. and C. W. Wicks, Jr., S–P conversion from the transition zone beneath Tonga and the nature of the 670 km discontinuity, *Geophys. J. Int.*, **101**, 1–35, 1990.

Shearer, P. M., Global mapping of upper mantle reflectors from long-period SS precursors, *Geophys. J. Int.*, **115**, 878–904, 1993.

Shearer, P. M. and T. G. Masters, Global mapping of topography on the 660 km discontinuity, *Nature*, **355**, 791–796, 1992.

van der Hilst, R., R. Engdahl, W. Spakman, and G. Nolet, Tomographic imaging of subducted lithosphere below north-west Pacific island arcs, *Nature*, **353**, 37–43, 1991.

van der Lee, S., H. Paulssen, and G. Nolet, Variability of P660s phases as a consequence of topography of the 660 km discontinuity, *Phys. Earth Planet. Inter.*, **86**, 147–164, 1994.

Vidale, J. E. and H. M. Benz, Upper-mantle seismic discontinuities and the thermal structure of subduction zones, *Nature*, **356**, 678–682, 1992.

Vinnik, L. P., Detection of waves converted from P to SV in mantle, *Phys. Earth Planet. Inter.*, **15**, 39–45, 1977.

Walck, M. C., The P-wave upper mantle shear structure beneath an active spreading center: The Gulf of California, *Geophys. J. R. Astron. Soc.*, **76**, 697–723, 1984.

Wicks, C. W., Jr. and M. A. Richards, A detailed map of the 660-kilometer discontinuity beneath the Izu-Bonin subduction zone, *Science*, **261**, 1424–1427, 1993.